Phys. Lett. B 851 (2024) 138559

Contents lists available at ScienceDirect

Physics Letters B

journal homepage: www.elsevier.com/locate/physletb

Letter

# Short-range correlations in dynamical intranuclear cascade models for describing nucleon knockout reactions

J.L. Rodríguez-Sánchez [a,b,*], J. Cugnon [c], J.C. David [d], J. Hirtz [d,e]

[a] CITENI, Campus Industrial de Ferrol, Universidade da Coruña, E-15403 Ferrol, Spain
[b] IGFAE, University of Santiago de Compostela, E-15782 Santiago de Compostela, Spain
[c] AGO department, University of Liège, allée du 6 août 19, bât. B5, B-4000 Liège, Belgium
[d] IRFU, CEA, Université Paris-Saclay, F-91191 Gif-sur-Yvette, France
[e] Physics Institute, University of Bern, Sidlerstrasse 5, 3012 Bern, Switzerland

ARTICLE INFO

Editor: A. Schwenk

*Keywords:*
Short-range nucleon-nucleon correlations
Knockout reactions
Intranuclear cascade models
INCL+ABLA

ABSTRACT

Spallation and fragmentation reactions at incident energies above the Fermi momentum are considered to be the main mechanism for the production of neutron-rich nuclei at worldwide nuclear physics facilities, such as RIBF, FRIB, and GSI-FAIR. Although it is widely known that dynamical reaction models give a rather good prediction of cross sections for nuclear residues produced in spallation and fragmentation reactions, these reaction models fail in the description of peripheral collisions involving short-range nucleon-nucleon correlations (SRCs). Here, we present state-of-the-art dynamical reaction calculations based on the intranuclear cascade approach to describe spallation and fragmentation reactions. The new version of our dynamical model, including SRCs, successfully describes isotopic cross sections of neutron-rich nuclear residues and inclusive single-neutron and single-proton knockout cross sections for various stable and exotic nuclei. Finally, the results show that the systematic strong dependency of the single-knockout cross section reduction factor on the neutron-proton separation energy asymmetry parameter ($\Delta S$) obtained by Tostevin and Gade disappears when SRCs are taken into account.

## 1. Introduction

Direct reactions have been one of the key experimental probes to build up our understanding of the nuclear shell structure [1]. At incident energies above the Fermi momentum spallation, fragmentation, and electron-nucleus reactions can populate hole states via nucleon-removing collisions [2] allowing for the study of states near the Fermi surface of stable and unstable nuclei, which were used in the pioneering works of Mayer and Haxel [3,4] to display the behavior of single-particle states. This fact motivates a simplified description of nuclei in terms of an independent-particle model (IPM), in which nucleons move freely in an average potential [5]. Traditionally, the deviations of the single-nucleon knockout cross sections from the simple IPM description have been quantified by high-energy electron scattering measurements on stable nuclei between $^{7}$Li and $^{208}$Pb [6], evidencing that the strength of dominant single-particle states, the so-called spectroscopic factor (SF), is reduced by about $30-40\%$ in comparison to predictions based on the IPM. This deviation can be understood as a consequence of the presence of nucleon-nucleon correlations, such as long- and short-range correlations (SRCs), where the latest might be induced by the short-range tensor interaction due to the exchange of $\rho$ and $\pi$ mesons [7,8]. Recently, state-of-the art calculations based on the effective pair-based generalized contact formalism and ab initio quantum Monte Carlo approaches have also shown that SRCs would be explained in terms of the mean-field approximation [9] as a long-range quantity that is independent of the short-distance nature of the nuclear force.

Experimentally, the first systematic study of single-nucleon knockout cross sections was carried out using high-energy electron scattering experiments, in which the scattered electrons and knockout nucleons were detected with high-resolution spectrometers [10,11], and showed that the SFs do not present any dependency on isospin or mass number [6]. This behavior has also been confirmed by other measurements based on proton and neutron transfer reactions, investigating more than 30 stable nuclei [12,13], and by quasi-free nucleon scattering reactions in inverse kinematics covering large ranges of isotopic chains [14–16], which have led to strong conclusions about the isospin independency quantified by the difference between single proton and neutron separation energies. This latter parameter is used as a measure of the

* Corresponding author at: CITENI, Campus Industrial de Ferrol, Universidade da Coruña, E-15403 Ferrol, Spain.
*E-mail address:* j.l.rodriguez.sanchez@udc.es (J.L. Rodríguez-Sánchez).

https://doi.org/10.1016/j.physletb.2024.138559
Received 28 May 2023; Received in revised form 20 February 2024; Accepted 1 March 2024
Available online 6 March 2024

asymmetry of the neutron and proton Fermi surfaces. In contrast, a recent compilation of existing single-nucleon knockout data by Tostevin and Gade [17,18] reports reduction factors relative to the shell model (SM) predictions for a large number of nuclei. Whereas the residual interactions in SM calculations can account for the spread of the single-particle strength near the Fermi surface, the findings obtained in Refs. [17,19,20] point out a very strong dependency of SFs on the neutron-to-proton asymmetry of nuclei.

The isospin dependency of SFs is still highly debated and is unsettled whether this is an indication of correlation effects missing in the SM calculations [21,22] or deficiencies in the reaction model missing dynamical effects and/or nuclear excitation contributions [23], which is usually based on the simple eikonal approximation [24] with shell-model effective interactions [25]. In this Letter, we utilize a microscopic dynamical reaction model to describe the proton-nucleus (spallation) and nucleus-nucleus (fragmentation) collisions induced in different stable and exotic nuclear systems given place to inclusive single-nucleon knockout cross sections. Our dynamical model includes experimental parameterizations of nucleon-nucleon interaction cross sections, phenomenological and optical potentials, Hartree-Fock-Bogoliubov parameterizations for target and projectile density profiles, Pauli blocking, cluster formation, and final state interactions. Additionally, we also consider other nuclear excitations that would contribute to the single-nucleon removal cross sections, which will be detailed later.

## 2. Theoretical framework

Spallation and fragmentation reactions are described within the latest C++ versions of the dynamical Liège intranuclear-cascade model (INCL) [26,27] coupled to the ablation model ABLA++ [28,29], which are based on Monte Carlo techniques obeying conservation laws throughout each reaction event [30]. INCL describes these reactions as a sequence of binary collisions between the nucleons (hadrons) present in the projectile and target nuclei, mainly in the geometrical overlapping region [31]. Nucleons move along straight trajectories until they undergo a collision with another nucleon or until they reach the surface, where they might eventually escape. INCL also includes isospin- and energy-dependent nucleus potentials calculated according to optical models [30], as well as isospin-dependent pion potentials [32] required for the description of inelastic nucleon-nucleon interactions exciting baryonic resonances [33,34]. Recently, INCL has been extended toward high energies (∼20 GeV) including new interaction processes, such as multipion production [35], production of $\eta$ and $\omega$ mesons [36], and strange particles [37–39], such as kaons and hyperons. At the first step of the simulation, projectile and target density profiles are prepared assuming independent Woods-Saxon density distributions for protons, neutrons, and Λ-particles (only used for hypernuclei) [30,38,40]. For the Woods-Saxon density distribution the radius ($R_0$) and the diffuseness parameter ($a$) are taken from Hartree-Fock-Bogoliubov calculations [41]. Additionally, the nucleons are sampled in phase space taking into account the correlations between kinetic energy and radius of the potential well [42], such that the relationship is given by the Woods-Saxon distribution. Therefore this new version of INCL allows us to predict the formation of spallation and fragmentation remnants and their characterization in atomic ($Z$) and mass ($A$) numbers, strangeness number, excitation energy, and angular momentum. We remark that the good agreement of INCL calculations with experimental neutron and proton emission production cross sections obtained from spallation-induced reactions on light, medium-mass, and heavy nuclei at energies from few MeV/u up to 20 GeV/u [26,30], as well as a reasonable description of isotopic cross sections [26,28,30], allow us to guarantee a correct prediction of the excitation energy gained by the remnants after the spallation and fragmentation reactions.

Assuming an inverse kinematics framework for the reaction description, SRCs are only considered for the projectile nucleus since experimentally this is the most investigated case in worldwide nuclear physics facilities, such as RIBF, FRIB, and GSI-FAIR. The implementation in INCL is based on the prescriptions given in Refs. [43,44]. At the beginning of each INCL event the nucleons are sampled inside the potential well, looking afterwards for neutron-proton (np) pairs since these correlations represent around 90% of the total amount of SRCs [43]. The nn and pp correlations are considered negligible and are not included in these calculations. Here we consider np pairs are formed when their inter-distance ($d_{max}$) is smaller than 1.6 fm, about twice the proton radius [45]. During the projectile-target collision, INCL looks for nucleon-nucleon interactions and if one of these SRC nucleons is involved in the collision, the interaction is modeled as a quasi-free two-nucleon knockout processes [44], assuming that all the participants move in the same reaction plane. The SRC kinematics is described as a back-to-back emission of the correlated nucleons in the center-of-mass of the colliding nucleons. Here it is essential to fix the value of the maximum momentum $P_{max}$ gained by the SRC nucleons. This parameter is constrained using the many-body nucleon momentum distribution $n(k)$ obtained from inclusive $A(e,e')X$ reactions performed with a $^{56}$Fe and $^{12}$C targets [10,46], as shown in Figs. 1(a) and 1(b) respectively, whose large momentum tail provides information about the amount and effects introduced by the SRC nucleons in the nuclear potential well [11,46–48]. One can see in the figure that the momentum tail increases with the value of $P_{max}$, as expected since the SRCs increase the momentum of the nucleons. We achieve the best agreement when $P_{max}$ is equal to twice the Fermi momentum (270 MeV/c). The value of $P_{max}$ is fixed in our model because we only have experimental data for the mentioned stable nuclei and, consequently, there is no avenue for further

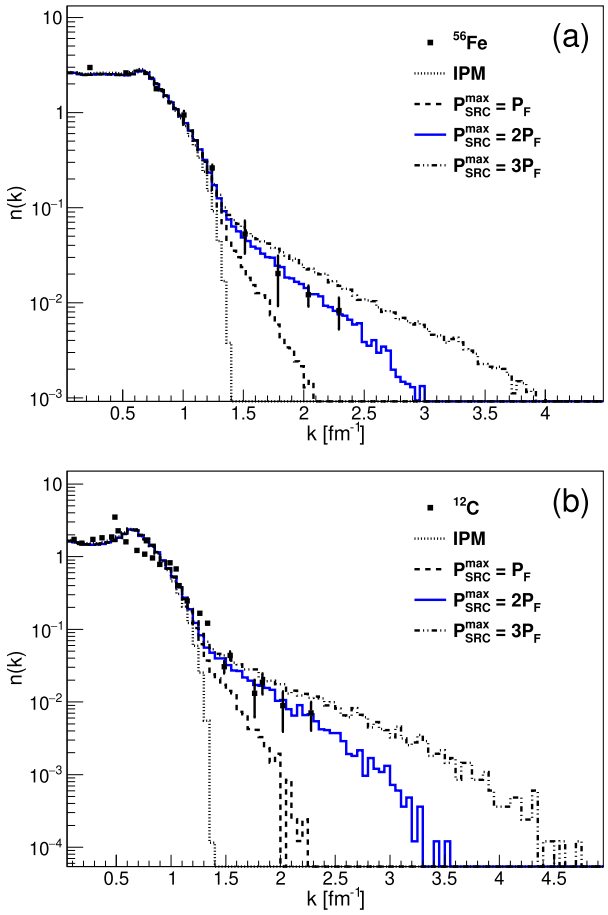


**Fig. 1.** The INCL predictions for the many-body nucleon momentum distribution $n(k)$ assuming different constraints for $P_{max}$ are compared to experimental values obtained from inclusive $A(e,e')X$ reactions for $^{56}$Fe (a) and $^{12}$C (b) targets [10,46].

constraint on this parameter for neutron-rich and/or neutron-deficient nuclear systems. Nonetheless, these results are in a reasonable agreement with the findings reported in Refs. [46,49,50] and we will see later that this approach works quite well. Then the SRC nucleons are marked as participants and propagated inside the projectile-like nucleus looking for collisions with the rest of spectators or escape from the nucleus. Prior to initiating the propagation process, the momentum coming from SRCs is added to the momentum of the SRC nucleons inside the potential well, under the assumption that the direction of the SRC breaking is the straight line connecting the centers of the two SRC nucleons. This assumption is introduced by considering the back-to-back emission and the need for conservation of momentum and energy. The additional SRC momentum is then sampled as a random value between zero and $P_{max}$, depending quadratically on the distance between the centers of the two nucleons ($d$) according to the equation: $P^{SRC} = x^2 P_{max}$, where $x = (d_{max} - d)/d_{max}$. Other dependencies on $x$ have also been used to describe the experimental data in Fig. 1, but only the quadratic dependency is able to reproduce the experimental data. If the two SRC nucleons run away without interacting with other nucleons, this channel will contribute as a two-nucleon knockout reaction populating mainly remnants with a mass equal to $A_{projectile} - 2$. Concerning Pauli blocking, during the propagation of these SRC nucleons, they are subject of statistical and strict Pauli blockings in order to guarantee the momentum and energy conservation at the end of the cascade process, as performed for normal nucleons [26,30,51]. Note that the momentum coming from SRCs is only added if the np pair is broken, otherwise the particle kinematics and their propagations are performed as usual.

For nucleus-nucleus collisions, apart from the fragmentation contribution, we also take into account in these calculations other excitations induced by the isovector giant dipole, isoscalar giant quadrupole (ISGQR), isovector giant quadrupole, and the double giant dipole resonances (GDR), whose main decay channels lead to the emission of neutrons and protons. The main contribution to nuclear excitations arises from the excitation of the ISGQR [52–54] that for the reactions studied in this work at kinetic energies of ∼100 MeV/u fluctuates between 30 and 150 mb, depending on the colliding nuclei.

INCL is then coupled to the deexcitation model ABLA++ [28] to determine the particle emission probabilities, which are calculated according to the Weißkopf-Ewing formalism [55]. For a more realistic description of the deexcitation process, the separation energies and the emission barriers for charged particles are calculated by using the atomic mass evaluation AME2020 [56] and the prescription given by Qu and collaborators [57], respectively. We use Qu's approach instead of the usual Bass model [58] because both descriptions provide similar results for the emission barriers, but Qu's approach is much faster in the case of intermediate-mass and heavy remnants.

## 3. Single-nucleon knockout reactions

It is well-known that correlations arising from short-range nucleon-nucleon interactions involving low-lying states result in a further reduction of the physical nucleon occupancies of states near the Fermi surface, being the associated single-particle strength shifted into a large number of states at higher energies [7,59,60]. This fact reduces the cross sections of single-nucleon knockout reactions and increases slightly the cross sections of lighter nuclear residues ($A-2$, $A-3$, ..., channels).

In Figs. 2(a) and 2(b) we display the inclusive single-proton removal cross sections (open circles) as a function of the projectile neutron excess ($N/Z$) for the isotopic chains of Si [61] and Sn [62,63], respectively. The experimental data are compared to our model calculations displaying the different contributions to the cross sections. Solid stars correspond to the contribution from the excitation of ISGQR and GDR resonances. For the excitation energy spectra of these reactions we assume a Lorentzian function, considering that the ISGQR states are located at $E_{ISGQR} = 62A^{-1/3}$ MeV with a width of $\sigma_E = 0.029E^{1.9}$ MeV [64]. As can be seen in the figures, this contribution (solid stars) is only important for nuclei close to $N/Z \sim 1$, where the proton separation energies are smaller than the neutron ones. This fact increases the cross section for the single-proton removal channel due to the proton emission during the deexcitation stage and the subsequent population of the single-proton removal channel.

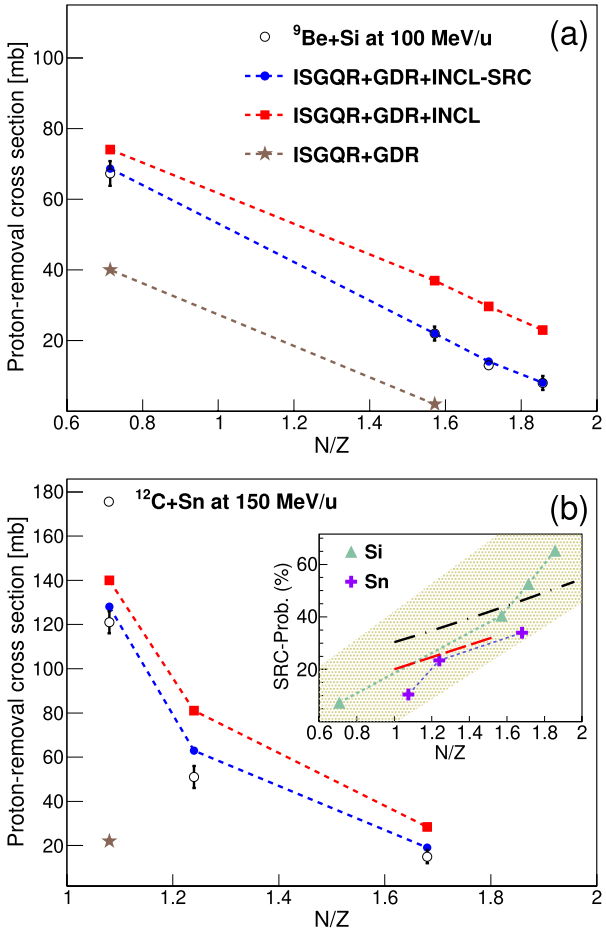


**Fig. 2.** Inclusive single-proton removal cross sections (open circles) as a function of the neutron excess ($N/Z$) for the isotopic chains of Si [61] (a) and Sn [62,63] (b). The lines with markers illustrate the different contributions to the experimental data, see text for details. It is worth noting that calculations are performed solely for the experimental data points, while the lines serve the purpose of visually guiding the eye. The inset shows the cross section reduction factor deduced in this work (solid triangles and crosses) due to the presence of SRC as a function of the neutron excess, which is compared to the results obtained by the CLAS collaboration [68] (long-dashed line), theoretical calculations from Ref. [69] (long dashed dotted line), and to the systematic given by Tostevin and Gade [17,18] (shaded area).

The contribution of the resonance excitations and INCL+ABLA (solid squares) is also shown. This calculation gives cross sections larger than the experimental data. Finally, we also display the results including SRCs (solid circles). In this case the SRCs reduce the cross sections a factor between 5 and 65% depending on the neutron excess as shown in the inset of Fig. 2(b), where the reduction factor in percent is calculated as: $100\times(1-\sigma^{INCL-SRC}/\sigma^{INCL})$ (solid triangles and crosses). In the inset the systematic trend derived by Tostevin and Gade [17,18] is also shown with a shaded area. As expected, the SRC contribution to the single-proton knockout channel is more important for larger neutron-to-proton asymmetries since the amount of correlated protons forming $np$ pairs increases with the neutron excess, as observed in high-energy electron scattering experiments [68]. The tendency obtained in Ref. [68] is also displayed with a long-dashed line. These results are also compared

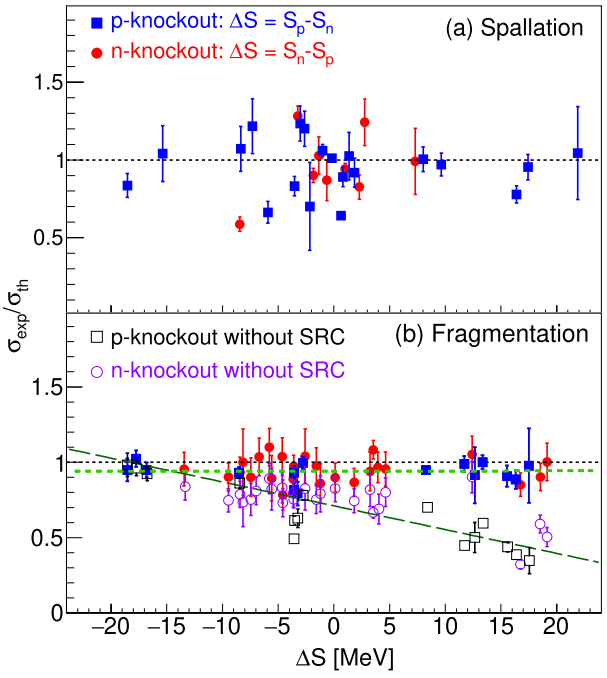


**Fig. 3.** Computed ratios of the experimental and theoretical inclusive single-nucleon-removal cross sections induced by spallation [14,41,62] (a) and fragmentation [62,63,65–67] (b) reactions as a function of the parameter $\Delta S$ defined in the upper part of the figure. The solid (empty) squares correspond to single-proton removal reactions while the solid (empty) circles are for single-neutron removal ones with (without) SRCs. The short- and long-dashed lines correspond to the fits with and without SRCs, respectively, and are shown just to guide the eye.

to the power law given in Ref. [69], where the number of correlated pairs scales with $\sim A^{1.44}$. This is illustrated by a long dashed dotted line assuming the isotopic chain of Sn and normalizing to the maximum number of pairs corresponding to $^{100}$Sn. All these findings are in a reasonable agreement considering the large range covered by the systematic trend given by Tostevin and Gade.

Clearly, the new version of INCL provides a better description of the evolution of the single-nucleon knockout cross section with the neutron excess. To go further in the Fig. 3 we systematically represent the ratio of the measured and theoretical cross sections ($\sigma_{exp}/\sigma_{th}$) as a function of the neutron-proton separation energy asymmetry parameter $\Delta S$ for spallation (a) and fragmentation (b) reactions measured in different works [14,16,41,62,63,65–67,70]. In both cases, the ratio is around the unit, with a larger dispersion between 0.5 and 1.3 for single-neutron and single-proton knockout in spallation reactions. This could be because there are few measurements, which have been performed in different experiments and conditions. For nucleon knockout induced by fragmentation reactions the dispersion is smaller, between 0.75 and 1.15. Here the calculations without SRCs are also displayed with empty symbols to show the dependency on the $\Delta S$ parameter. Therefore, from these results, we conclude that after including the SRC channel the ratios do not dependent on the neutron-to-proton asymmetry, as recently obtained in different experimental and theoretical investigations [14,70–76]. This good agreement demonstrates that the SRC reaction channel and its dynamics are very relevant to describe properly single-nucleon knockout reactions.

## 4. Multiple-nucleon knockout reactions

The emission of the two SRC nucleons populates directly the nuclear residues with mass $A-2$, while the nuclear residues with masses $A-3$, $A-4$, ..., are populated due to the re-scattering with other nucleons inducing their emission. This effect can be observed in Fig. 4 where

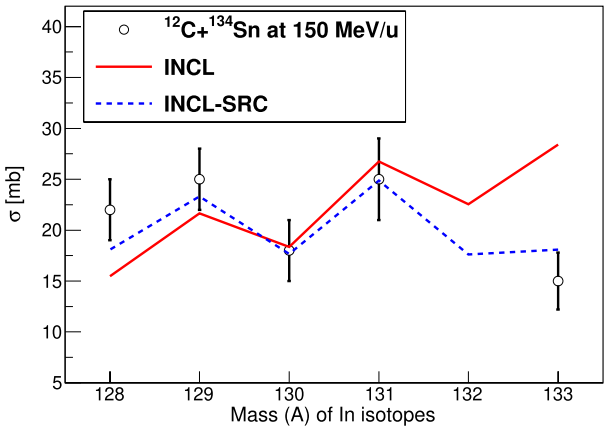


**Fig. 4.** Cross sections for In isotopes produced after the removal of a single proton and several neutron in the reaction $^{134}$Sn (150 MeV/u) impinging onto a $^{12}$C target (open circles) [63]. The data is compared to standard INCL (solid line) and INCL-SRC (dashed line) calculations.

standard INCL (solid line) and INCL-SRC (dashed line) calculations are compared to isotopic cross sections of In isotopes produced in the reaction $^{134}$Sn (150 MeV/u) impinging onto a $^{12}$C target [63]. In the case of the single-proton removal channel ($A=133$) the cross section decreases because of SRCs, while the others change slightly. The main discrepancy is found for the In isotope $A=128$, although this occurs for both calculations.

Surprising, this new approach combining INCL and contributions from resonance excitations seem to be in very good agreement with the results obtained in high-energy electron scattering experiments [68] and recent spectroscopic factor studies [12,14,70–73]. Moreover, we also get a better description of isotopic cross sections related to the nuclear residues with masses $A-2$, $A-3$, $A-4$, ..., that can be populated due to the excitation energy introduced by the breaking of the n-p pairs as well as their additional re-scattering.

## 5. Summary and conclusions

The dynamical intranuclear cascade model INCL has been improved by including short-range nucleon-nucleon correlations dominated mainly by the formation of *np* pairs. This new development allows us to get a better description of pheripheral collisions involving the knockout of few nucleons in spallation and fragmentation reactions.

In Fig. 2 we have demonstrated that for the description of knockout reactions at intermediate kinetic energies (~150 MeV/u) isoscalar giant quadrupole and double giant dipole resonances are required to reproduce the inclusive single-proton knockout cross sections measured for the Si and Sn isotopic chains, where the SRCs reduce the knockout cross sections by a factor of around 5% for symmetric nuclei and about 65% for highly asymmetry nuclei. It is clear that the SRCs reduce the cross sections almost linearly with the neutron excess, as already pointed out recently by high-energy electron scattering experiments [68].

After including the SRCs, the calculated ratios of the experimental and theoretical inclusive single-nucleon removal cross sections induced by spallation and fragmentation reactions as a function of the projectile asymmetry in terms of the neutron-proton separation energy parameter seem to indicate an independence on the neutron-to-proton asymmetry. This allows to reconcile the theoretical calculations of nucleon knockout reactions with those obtained through nucleon transfer [12,13] as well as high-energy electron scattering [6,10,11,68] reactions. Our results also demonstrate that the SRC reaction channel and its dynamics play an important role to describe properly single-nucleon knockout reactions, as can also be deduced from the comparison of intermediate-energy single-nucleon removal cross section measurements with shell model calculations [17–19]. It should be noted that the SRC effects ob-

tained for the single-nucleon knockout cross sections studied in this Letter are smaller than 65%, which is in clear agreement with the values reported by the CLAS collaboration [68] and in Refs. [17,19], although in the latter the SRC contribution for the most strongly bound states can reach a percentage of 80%.

Finally, we would also like to note that the measurement of single and multiple nucleon knockout cross sections for a large range of a given isotopic chain, as shown in Figs. 2 and 4, in coincidence with the kinematics of the emitted nucleons is crucial for further insight into SRCs. This kind of measurement can be easily performed in inverse kinematics experiments [77] at worldwide nuclear physics facilities, such as RIBF, FRIB, and GSI-FAIR. However, due to the re-scattering of the outgoing nucleons with the remnant in inverse kinematics, the emitted nucleons can much more easily populate the large momentum tail observed in Ref. [68], making it more difficult to disentangle the SRC nucleons from the re-scattered ones. To solve this possible issue, we would propose to simultaneously measure the $\gamma$-rays emitted during the deexcitation stage since the SRC pairs could populate forbidden excited states [78–80]. The combination of complete kinematic measurements of nuclear residues, high-momentum nucleons, and $\gamma$-ray spectroscopy could provide a powerful tool for advancing our understanding of the behavior of nucleon-nucleon interactions in nuclear matter under extreme conditions.

## Declaration of competing interest

The authors declare that they have no known competing financial interests or personal relationships that could have appeared to influence the work reported in this paper.

## Acknowledgements

We thank Dr. A. Boudard, Dr. D. Mancusi and Dr. S. Leray for enlightening discussions and Prof. C. A. Bertulani for providing us with the total ISGQR and GDR cross sections. This work was partly supported by the P2IO LabEx (ANR-10-LABX-0038) in the framework “Investissements d’Avenir” (ANR-11-IDEX-0003-01), managed by the Agence Nationale de la Recherche (ANR) (France). J.L.R.-S. is thankful for the support provided by the Regional Government of Galicia under the Postdoctoral Fellowship Grant No. ED481D-2021/018 and under the program “Proyectos de excelencia” Grant No. ED431F-2023/43, and by the “Ramón y Cajal” program under Grant No. RYC2021-031989-I funded by MCIN/AEI/10.13039/501100011033 and “European Union NextGenerationEU/PRTR”.

## References

[1] Hannah B. Burrows, W.M. Gibson, J. Rotblat, Phys. Rev. 80 (1950) 1095.
[2] G. Jacob, Th.A.J. Maris, Rev. Mod. Phys. 38 (1966) 121.
[3] M.G. Mayer, Phys. Rev. 75 (1949) 1969.
[4] O. Haxel, J.H.D. Jensen, H.E. Suess, Phys. Rev. 75 (1949) 1766.
[5] I. Sick, Prog. Part. Nucl. Phys. 59 (2007) 447.
[6] L. Lapikás, Nucl. Phys. A 553 (1993) 297.
[7] W. Dickhoff, C. Barbieri, Prog. Part. Nucl. Phys. 52 (2004) 377.
[8] T. Otsuka, et al., Phys. Rev. Lett. 95 (2005) 232502.
[9] R. Cruz-Torres, et al., Nat. Phys. Lett. 17 (2021) 306.
[10] D.B. Day, et al., Phys. Rev. Lett. 59 (1987) 427.
[11] O. Hen, et al., Rev. Mod. Phys. 89 (2017) 045002.
[12] B.P. Kay, et al., Phys. Rev. Lett. 111 (2013) 043502.
[13] J.P. Schiffer, et al., Phys. Rev. Lett. 108 (2012) 022501.
[14] L. Atar, et al., The R$^3$B Collaboration, Phys. Rev. Lett. 120 (2018) 052501.
[15] M. Gómez-Ramos, A.M. Moro, Phys. Lett. B 785 (2018) 511.
[16] N. Paul, et al., Phys. Rev. Lett. 122 (2019) 162503.
[17] J.A. Tostevin, A. Gade, Phys. Rev. C 90 (2014) 057602.
[18] J.A. Tostevin, A. Gade, Phys. Rev. C 103 (2021) 054610.
[19] A. Gade, et al., Phys. Rev. C 77 (2008) 044306.
[20] P.G. Hansen, J.A. Tostevin, Annu. Rev. Nucl. Part. Sci. 53 (2003) 219.
[21] N.K. Timofeyuk, Phys. Rev. C 88 (2013) 044315.
[22] R. Cruz-Torres, et al., Phys. Lett. B 785 (2018) 304.
[23] C.A. Bertulani, Y. Kucuk, R. Lozeva, Phys. Rev. Lett. 124 (2020) 132301.
[24] C. Bertulani, A. Gade, Comput. Phys. Commun. 175 (2006) 372.
[25] S. Cohen, D. Kurath, Nucl. Phys. 73 (1965) 1.
[26] D. Mancusi, A. Boudard, J. Cugnon, J.-C. David, P. Kaitaniemi, S. Leray, Phys. Rev. C 90 (2014) 054602.
[27] J.-C. David, I. Leya, Prog. Part. Nucl. Phys. 109 (2019) 103711.
[28] J.L. Rodríguez-Sánchez, J. Cugnon, J.-C. David, J. Hirtz, A. Kelić-Heil, S. Leray, Phys. Rev. C 105 (2022) 014623.
[29] J.L. Rodríguez-Sánchez, J. Cugnon, J.-C. David, J. Hirtz, A. Kelić-Heil, I. Vidaña, Phys. Rev. Lett. 130 (2023) 132501.
[30] A. Boudard, J. Cugnon, J.-C. David, S. Leray, D. Mancusi, Phys. Rev. C 87 (2013) 014606.
[31] J. Cugnon, et al., Nucl. Instrum. Methods Phys. Res. B 111 (1996) 215.
[32] Th. Aoust, J. Cugnon, Phys. Rev. C 74 (2006) 064607.
[33] J.L. Rodríguez-Sánchez, et al., Phys. Lett. B 807 (2020) 135565.
[34] J.L. Rodríguez-Sánchez, et al., Phys. Rev. C 106 (2022) 014618.
[35] D. Mancusi, S. Lo Meo, N. Colonna, A. Boudard, M.A. Cortés-Giraldo, J. Cugnon, J.-C. David, S. Leray, J. Lerendegui-Marco, C. Massimi, V. Vlachoudis, Eur. Phys. J. A 53 (2017) 80.
[36] J.-C. David, A. Boudard, J. Cugnon, J. Hirtz, S. Leray, D. Mancusi, J.L. Rodríguez-Sánchez, Eur. Phys. J. Plus 133 (2018) 253.
[37] J. Hirtz, J.-C. David, A. Boudard, J. Cugnon, S. Leray, D. Mancusi, Eur. Phys. J. Plus 133 (2018) 436.
[38] J.L. Rodríguez-Sánchez, J.C. David, J. Hirtz, J. Cugnon, S. Leray, Phys. Rev. C 98 (2018) 021602(R).
[39] J. Hirtz, J.-C. David, A. Boudard, J. Cugnon, S. Leray, I. Leya, J.L. Rodríguez-Sánchez, G. Schnabel, Phys. Rev. C 101 (2020) 014608.
[40] H.D. Vries, C.W.D. Jager, C.D. Vries, At. Data Nucl. Data Tables 36 (1987) 495.
[41] J.L. Rodríguez-Sánchez, et al., Phys. Rev. C 96 (2017) 054602 and references therein.
[42] A. Boudard, J. Cugnon, S. Leray, C. Volant, Phys. Rev. C 66 (2002) 044615.
[43] R. Subedi, et al., Science 320 (2008) 1476.
[44] S. Stevens, et al., Phys. Lett. B 777 (2018) 374.
[45] W. Vassen, Science 358 (2017) 39.
[46] C. Ciofi degli Atti, S. Simula, Phys. Rev. C 53 (1996) 1689.
[47] S. Terashima, et al., Phys. Rev. Lett. 121 (2018) 242501.
[48] J. Ryckebusch, W. Cosyn, T. Vieijra, C. Casert, Phys. Rev. C 100 (2019) 054620.
[49] C. Ciofi degli Atti, Phys. Rep. 590 (2015) 1.
[50] R. Schiavilla, et al., Phys. Rev. Lett. 98 (2007) 132501.
[51] J. Cugnon, et al., Nucl. Phys. A 620 (1997) 475.
[52] M.B. Lewis, F.E. Bertrand, Nucl. Phys. A 196 (1972) 337.
[53] G. Satchler, Nucl. Phys. A 472 (1987) 215.
[54] C.A. Bertulani, Phys. Rev. Lett. 94 (2005) 072701.
[55] V.F. Weisskopf, D.H. Ewing, Phys. Rev. 57 (1940) 472.
[56] W.J. Huang, M. Wang, F.G. Kondev, G. Audi, S. Naimi, Chin. Phys. C 45 (2021) 030002.
[57] W.W. Qu, et al., Nucl. Phys. A 868 (2011) 1.
[58] R. Bass, in: Proceedings of the Symposium on Deep-Inelastic and Fusion Reactions with Heavy Ions, Springer Verlag, Berlin, 1980.
[59] V.R. Pandharipande, I. Sick, P.K.A. de Witt Huberts, Rev. Mod. Phys. 69 (1997) 981.
[60] D. Rohe, et al., Phys. Rev. Lett. 93 (2004) 182501.
[61] S.R. Stroberg, et al., Phys. Rev. C 90 (2014) 034301.
[62] L. Audirac, et al., Phys. Rev. C 88 (2013) 041602(R).
[63] V. Vaquero, et al., Phys. Lett. B 795 (2019) 356.
[64] C.A. Bertulani, G. Baur, Phys. Rep. 163 (1988) 299.
[65] J.L. Rodríguez-Sánchez, et al., Phys. Rev. C 96 (2017) 034303.
[66] J. Díaz-Cortés, et al., Phys. Lett. B 811 (2020) 135962.
[67] J.M. Boillos, et al., The R$^3$B Collaboration, Phys. Rev. C 105 (2022) 014611.
[68] M. Duer, et al., Nature 560 (2018) 617.
[69] M. Vanhalst, W. Cosyn, J. Ryckebusch, Phys. Rev. C 84 (2011) 031302(R).
[70] M. Holl, et al., Phys. Lett. B 795 (2019) 682.
[71] S. Kawase, et al., Prog. Theor. Exp. Phys. 2018 (2018) 021D01.
[72] S. Paschalis, M. Petri, A.O. Macchiavelli, O. Hen, E. Piasetzky, Phys. Lett. B 800 (2020) 135110.
[73] F. Flavigny, et al., Phys. Rev. Lett. 110 (2013) 122503.
[74] Ø. Jensen, G. Hagen, M. Hjorth-Jensen, B.A. Brown, A. Gade, Phys. Rev. Lett. 107 (2011) 032501.
[75] C. Barbieri, W.H. Dickhoff, Int. J. Mod. Phys. A 24 (2009) 2060.
[76] T. Aumann, et al., Prog. Part. Nucl. Phys. 118 (2021) 103847.
[77] M. Patsyuk, et al., The BM@N Collaboration, Nat. Phys. 17 (2021) 693.
[78] Takayuki Myo, Kiyoshi Kato, Hiroshi Toki, Kiyomi Ikeda, Phys. Rev. C 76 (2007) 024305.
[79] H.J. Ong, I. Tanihata, A. Tamii, et al., Phys. Lett. B 725 (2013) 277.
[80] Y.P. Xu, D.Y. Pang, X.Y. Yun, S. Kubono, C.A. Bertulani, C.X. Yuan, Phys. Rev. C 98 (2018) 044622.